Erschienen in: IEEE Journal of Photovoltaics ; 11 (2021), 4. - S. 967-973
https://dx.doi.org/10.1109/JPHOTOV.2021.3075850

On the Role of AlO_x Thickness in AlO_x/SiN_y: H Layer Stacks Regarding Light- and Elevated Temperature-Induced Degradation and Hydrogen Diffusion in c-Si

Andreas Schmid, Christian Fischer, Daniel Skorka, Axel Herguth, Clemens Winter, Annika Zuschlag, and Giso Hahn

***Abstract*—Light- and elevated temperature-induced degradation (LeTID) is assumed to be triggered by the hydrogen content in the crystalline silicon bulk. This article investigates differently thick atomic layer-deposited aluminum oxide (AlO_x) layers acting as diffusion barrier for hydrogen originating from a hydrogen-rich silicon nitride (SiN_y:H) layer. We demonstrate that the extent of LeTID can be significantly reduced by adjusting the AlO_x layer thickness up to 25 nm. To directly measure the diffusing species, a deuterium-rich SiN_y:D layer is deposited and the deuterium content is measured in an amorphous Si layer at the back side of the wafer via secondary ion mass spectrometry. Thus, a diffusion length of deuterium in the AlO_x layer of (3.8 ± 1.6) nm is determined at a firing temperature of $(743 \pm 2)^\circ$C. These results are not only a contribution to determine the LeTID formation dynamics, but also can be used to control LeTID in silicon wafers and solar cells.**

***Index Terms*—Aluminum oxide (AlO_x), degradation, deuterium, hydrogen, light- and elevated temperature-induced degradation (LeTID), secondary ion mass spectrometry (SIMS), silicon nitride (SiN_y:H).**

I. Introduction

LIGHT- and elevated temperature-induced degradation (LeTID [1]) is known to negatively impact the high-efficiency passivated emitter and rear cell concept, as first observed in multicrystalline silicon (mc-Si) [2]. It has been shown that LeTID can cause an efficiency loss of up to $10\%_{\mathrm{rel}}$ on cell level already during the first several hundred hours of illumination (depending on temperature and injection conditions) [1] but also impacts effective minority charge carrier lifetime (τ_{eff}) samples [3], [4] and may be followed by a phase of regeneration. The observed effect cannot be described by the boron-oxygen (BO) related degradation or FeB pair dissociation [2], [5]. It has been proven that LeTID occurs in both B- and Ga-doped mc-Si [2], [6], and further that Czochralski-grown (Cz) and float zone (FZ) Si materials are also affected by this kind of defect [7]–[10]. As in Cz-Si the BO defect formation also leads to a severe reduction of τ_{eff}, both degradation phenomena are usually measured in parallel, but recent studies already showed a way to identify the dominant defect [11].

Even though the underlying mechanisms of LeTID are still largely unknown, it could be shown that the kinetics are influenced by measurement conditions, like illumination and temperature (e.g., [1], [6]). In addition, (high-temperature) fabrication steps during sample processing like previous gettering steps [12] or the peak firing temperature [4], [8], [13]–[15] do also impact the extent of LeTID. While Kersten *et al.* [1] demonstrated that LeTID was only observed on samples passivated with hydrogen-containing dielectric layers during firing, Vargas *et al.* [16] showed that the severity of LeTID correlates with the amount of hydrogen released from the dielectric layer (into the atmosphere and/or into the c-Si) during firing which was further verified by studies of Bredemeier *et al.* [17] and Schmidt *et al.* [18].

Recently, many research groups were working on understanding the root cause of LeTID and tried to establish a defect model [4], [19]–[23]. However, the active elements forming the defect and being responsible for the defect formation have not yet been clearly identified. Bredemeier *et al.* [24] assumed a movement of impurities toward the wafer surface as the mechanism of regeneration. Based upon variations in wafer thickness, they identified cobalt and nickel due to their matching diffusion coefficients as potential candidates. In addition, they also considered hydrogen diffusing from the surface into the bulk and subsequently passivating bulk defects as a possible mechanism. Besides other investigations on the involvement of metallic impurities [20], [25]–[30], there is a growing recognition that hydrogen is involved in the defect formation [14], [17], [19], [21], [22], [26], [28], [31]–[33].

To determine the influence of hydrogen on the LeTID formation dynamics, the manipulation and measurement of the hydrogen content in the c-Si bulk gains more and more importance.

This work was supported in part by the German Federal Ministry of Economic Affairs and Energy under Grant FKZ 0324204B. *(Corresponding author: Andreas Schmid.)*

The authors are with the University of Konstanz, D-78457 Konstanz, Germany (e-mail: andreas.schmid@uni-konstanz.de; christian.fischer@uni-konstanz.de; daniel.skorka@uni-konstanz.de; axel.herguth@uni-konstanz.de; clemens.winter@uni-konstanz.de; annika.zuschlag@uni-konstanz.de; giso.hahn@uni-konstanz.de).

Konstanzer Online-Publikations-System (KOPS)
URL: http://nbn-resolving.de/urn:nbn:de:bsz:352-2-479vfjor46648

Varshney *et al.* [34] showed that LeTID severity gets stronger by depositing an AlO_x layer on top of the SiN_y:H layer and can be weakened by adding the AlO_x layer beneath. More recently, we showed that by varying the AlO_x thickness beneath the SiN_y:H layer, LeTID strength can be adjusted as well [35]. These findings could be explained by AlO_x acting as gas diffusion barrier [36] and thus reducing the in-diffusion of hydrogen in the c-Si bulk, which could also explain the effects observed on regeneration kinetics of the BO-related defect [37]. Based upon the works on the formation and dissociation of hydrogen dimers in silicon of Voronkov *et al.* [38] and subsequent studies [39], Helmich *et al.* [40] investigated the diffusion of hydrogen through the AlO_x layer by determining the boron-hydrogen concentration [BH] in the c-Si bulk. By varying the AlO_x thickness, they were able to indirectly identify diffusion lengths of hydrogen in the AlO_x layer being dependent on the firing peak temperature.

So far, all investigations on this topic were done by indirect measurements or evidence. In this study, the diffusing species is measured directly via secondary ion mass spectrometry (SIMS) measurements dependent on the AlO_x layer thickness within the AlO_x/SiN_y:H layer system with regard to its impact on lifetime evolution and the extent of LeTID at 130°C and 1-sun illumination.

II. Experimental

A. Lifetime Sample Preparation

Lifetime samples were processed using 1.2 Ωcm p-type boron-doped high-performance multicrystalline (hp mc) as well as 2.0 Ωcm p-type boron-doped Czochralski (Cz)-grown silicon sister wafers. All wafers were cut into 5 × 5 cm^2 samples and saw damage etched in a solution of HNO_3 (65%), CH_3COOH (99.8%), and HF (50%) in a ratio of 15:2.5:1, so that the final wafer thickness is approx. 160 ± 10 μm. Subsequently, an oxide was grown wet-chemically in a solution of H_2O_2 (30%) and H_2SO_4 (96%) in a ratio of 1:3 at about 80°C, which was afterwards stripped in diluted HF (3%) to remove surface contamination (Piranha clean). Aluminum oxide (AlO_x) was deposited at 300 °C on both sides of the samples using atomic layer deposition (ALD) in a *FlexAl-Reactor* (Oxford Instruments), in which the hydrogen concentration is relatively low (typically $<$ 1 atom%) [41]. The AlO_x layer thickness was varied between 0 and 25 nm. Furthermore, the samples were divided into subgroups as can be seen in Fig. 1. Group A received ALD AlO_x layers processed with variable hold time, hence with varying deposition times between several minutes and one hour. As deposition time at 300°C might play a role for the later observed LeTID kinetics, Group B was processed such that the temperature load at 300°C was identical for all samples of this group (31.5 min per side), and only the AlO_x layer thickness was varied by adjusting the number of deposition cycles. Furthermore, Group C was treated for 24 h at 400°C in an inert atmosphere at low pressure directly after AlO_x deposition, to potentially outgas hydrogen present in the AlO_x layer.

All samples then received a (75 ± 5) nm thick SiN_y:H layer by direct plasma-enhanced chemical vapor deposition (PECVD) at 450°C in a tool from centrotherm. Afterwards, firing was done in a belt furnace at a set peak temperature of 800°C. The temperature profiles of the samples during firing were measured via a temperature tracker (*DQ1860* from Datapaq) in combination with a type-K thermocouple (*HKMQIN-IM025U-500* from Omega) that is pressed on top of the wafer.

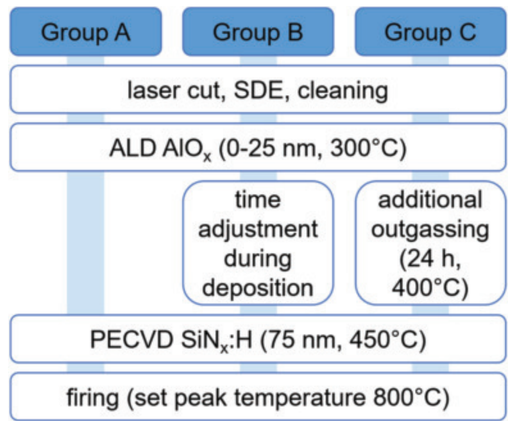

Fig. 1. Simplified process sequence of the investigated lifetime samples with the process variations during/after ALD AlO_x deposition.

Initial measurements of τ_{eff} have been carried out with a Sinton Instruments lifetime tester *WCT-120* at 30°C using the photoconductance decay (PCD) method [42]. For degradation and subsequent regeneration studies, the wafers were held at a temperature of approx. 130°C under illumination with halogen lamps (1.0 ± 0.1 suns) [43]. Here, τ_{eff} was measured *in situ* and repetitively at elevated treatment temperature on a PCD measurement tool with a temperature-controlled stage (Sinton Instruments lifetime tester *WCT-120TS*). During the *in situ* measurement, the halogen lamps are switched off automatically to not influence τ_{eff}. The lifetimes are extracted at a fixed excess charge carrier concentration of $\Delta n = 0.1 \cdot p_0$, where p_0 is the doping concentration of the investigated sample. To compare LeTID kinetics of various samples with varying τ_{eff} starting values, the lifetime equivalent defect density ΔN_{leq} [44] was calculated using

$$\Delta N_{\text{leq}} = \frac{1}{\tau_{\text{eff},t}} - \frac{1}{\tau_{\text{eff},0}} \tag{1}$$

where $\tau_{\text{eff},t}$ and $\tau_{\text{eff},0}$ are the extracted lifetime at any given time and in the initial state (after firing and illumination for 30 s to split FeB pairs), respectively. Note that for B-doped Cz material, a combination of BO-related degradation and LeTID is measured, while for higher firing temperatures (as applied in this work), LeTID is the dominating degradation mechanism [11].

The PECVD SiN_y:H layers were analyzed by Fourier-transform infrared spectroscopy (FT-IR) at room temperature using a *Vertex 80* from Bruker Optics in the spectral range of 500–4000 cm^{-1} with a resolution of 4 cm^{-1} and averaging over 50 spectra. The calculation of the hydrogen concentration in the layers was done according to [45], [46], using the N-H-related vibration mode at 3340 cm^{-1} and the Si-H-related vibration mode at 2200 cm^{-1}.

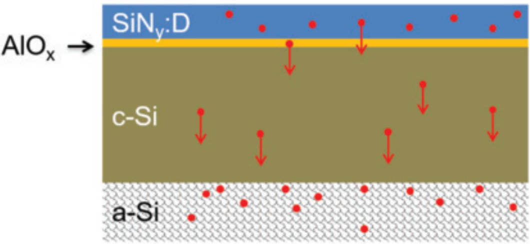

Fig. 2. Schematic representation of the sample structure for diffusion analysis (not to scale). Red dots symbolize deuterium.

B. Sample Preparation for Diffusion Analysis

For investigating hydrogen or deuterium diffusion in Si, respectively, 200 Ωcm p-type boron-doped float zone (FZ) silicon wafers with a thickness of (250 ± 10) μm were processed. After a short dip in HF (3%) to etch back the thin chemically grown oxide by the manufacturer, an ALD AlO_x layer was deposited at 300°C only on the front side of the wafer. The layer thickness was varied between 0 and 20 nm with variable hold times during deposition (see Group A, Fig. 1). On top, (85 ± 5) nm SiN_y:H/D was deposited using silane (SiH_4) and deuterated ammonia (ND_3) as precursors for direct PECVD in a laboratory scale reactor (*PlasmaLab 100* from Oxford Instruments) at 400°C (labeled SiN_y:D in the following). Radiofrequency magnetron sputtering of a pure-Si target without intentional heating was used to deposit 1.5 μm hydrogen-free amorphous Si (a-Si) [47] on the rear side of the wafer to trap deuterium, which is released from the SiN_y:D layer during firing and diffuses through the AlO_x and the c-Si substrate [48]. A schematic structure of the resulting samples is outlined in Fig. 2.

The samples were fired in a belt furnace, with the firing peak temperature set to 850°C. The temperature profiles of the samples during firing were measured as described in Section II-A. SIMS measurements of deuterium profiles were performed in the a-Si layer with a *Cameca ims4f-E6* using a caesium primary ion beam. The surface roughness of the FZ-Si wafers after the HF dip was determined using an atomic force microscope (AFM, MFP-3D from Asylum Research).

As an alternative second analysis method for the quantification of hydrogen/deuterium penetrating the AlO_x layer, the change in resistivity of the silicon substrate due to the formation of boron–hydrogen pairs ($B^- + H^+ \rightarrow BH$) [49] was investigated as described in [38], [39]. However, in our case, we used the direct resistivity measurement as described in [50] in more detail on identically processed samples as for the SIMS measurement. To trigger BH pair formation dynamics, the samples were annealed at approx. 180°C in the dark and the change in resistivity was monitored by *ex situ* measurements at 25°C.

III. Results and Discussion

A. Light- and Elevated Temperature-Induced Degradation

PCD measurements of the initial lifetime at room temperature directly after the firing step are shown in the upper graph of Fig. 3. Since sample temperature during firing has previously been shown to impact LeTID [4], [8], [13]–[15], the lower graph

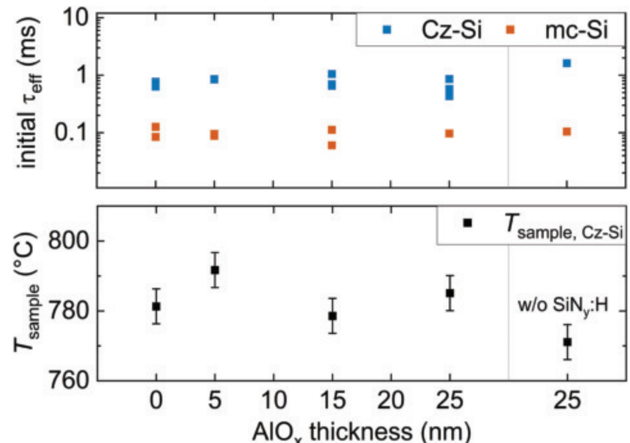

Fig. 3. Initial τ_{eff} measured by PCD at 30°C ($\Delta n = 0.1 \times p_0$) of all mc- and Cz-Si samples (top). Maximum sample temperature during firing (T_{set}= 800°C) of Cz-Si samples (bottom) with the systematic error of the temperature tracker and thermoelement. Both graphs are plotted against the AlO_x thickness within the AlO_x/SiN_y layer system.

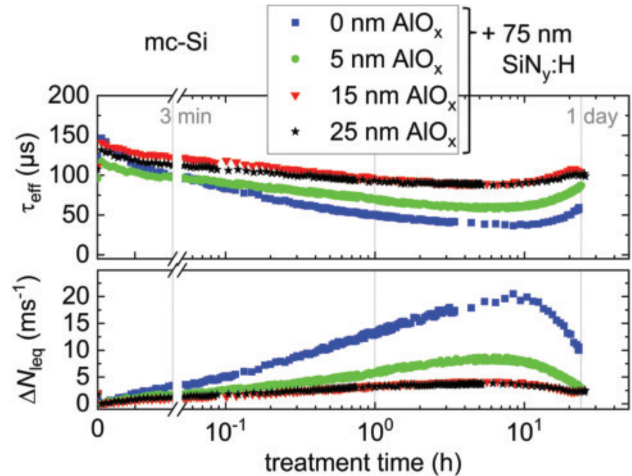

Fig. 4. Effective carrier lifetime (top) and equivalent defect density (bottom) of mc-Si lifetime samples passivated with AlO_x of different thickness and subsequent 75 nm SiN_y:H. τ_{eff} are extracted PCD lifetimes at elevated temperature at $\Delta n = 0.1 \times p_0$ and ΔN_{leq} is calculated according to (1) (x-axis: 0–3 min linear scale, subsequent log scale).

in Fig. 3 shows the sample peak temperature during firing at a set peak temperature of 800°C of Cz-Si samples with varying AlO_x layer thickness. It can be seen that the temperatures of samples with an AlO_x/SiN_y:H layer system are within the range of 779°C–792°C and the peak temperature of the sample without a final SiN_y:H layer is slightly lower at about 771°C.

As can be seen in the upper graph in Fig. 4, all investigated mc-Si samples show the typical LeTID and regeneration behavior. Within the first few hours at 130°C and 1-sun illumination, τ_{eff} decreases until it reaches its minimum after about 8–10 h and the regeneration sets in. As the starting values of τ_{eff} vary slightly between 100 and 150 μs, ΔN_{leq} is calculated according to (1) and is shown in the lower graph in Fig. 4. It can be clearly seen that the sample with solely SiN_y:H suffers most from LeTID. By adding an intermediate layer of 5 nm AlO_x, the maximum value of ΔN_{leq} can already be reduced by half. By

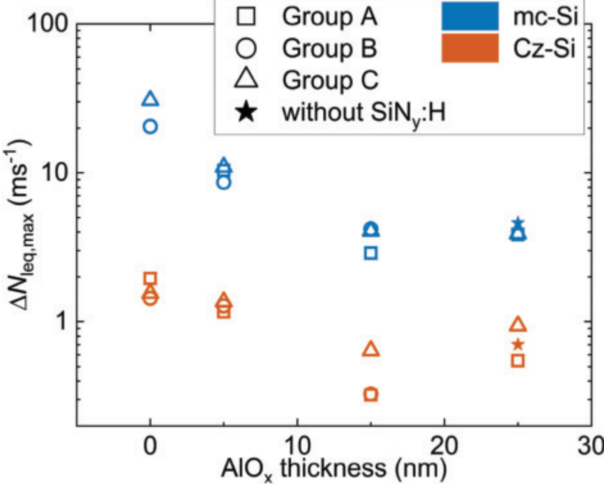

Fig. 5. Maximum values of the lifetime equivalent defect density of mc (blue) and Cz-Si (orange) versus the aluminum oxide thickness. In addition to the process with variable hold time during AlO_x deposition (Group A), a time adjustment during AlO_x deposition (Group B) and an outgassing of hydrogen after the AlO_x deposition (Group C) was applied. All samples—except the ones marked with a star—received a 75 nm SiN_y:H capping layer.

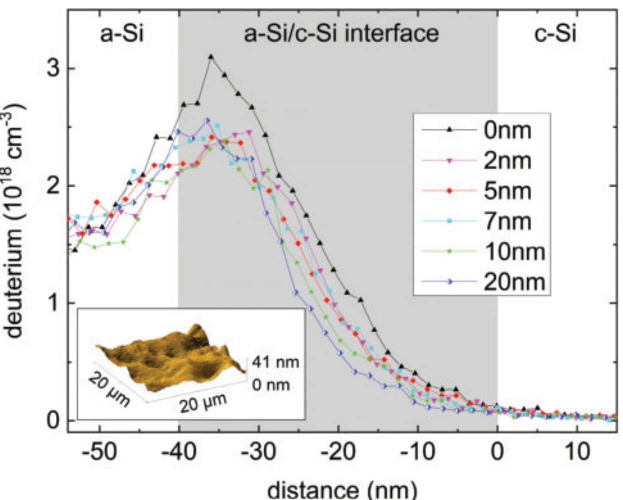

Fig. 6. Deuterium concentration dependent on SIMS sputter depth of all investigated samples. The inlay shows an AFM measurement of a FZ-Si surface after HF dip.

adding even thicker AlO_x layers of 15 nm, $\Delta N_{leq,max}$ can be lowered down to less than 5 ms^{-1}. Apparently, this value cannot be decreased further by increasing the AlO_x thickness to 25 nm but remains constant. The Cz-Si samples (not shown) exhibit a similar behavior under the same treatment conditions (130°C, 1-sun illumination), however, with lower $\Delta N_{leq,max}$ values (see Fig. 5). In literature, it has been shown that by changing the sample temperature during firing from 815°C to 744°C, a change in ΔN_{leq} of about 50% is expected (both in mc-Si and c-Si) [8]. Thus, it can be concluded that the slight temperature variations during firing obtained in this work are likely not responsible for the observed variations in maximal defect density during LeTID.

FT-IR measurements (on three samples passivated with solely SiN_y:H) show a decrease of the hydrogen concentration in the PECVD SiN_y:H layers after firing of 15–18%, which is consistent with the findings of Lindroos *et al.* [51] for comparable SiN_y:H layers deposited at 450°C. But from these results, it is not yet clear whether the hydrogen out-diffuses into the ambient or also in-diffuses into the c-Si wafer. Assuming that the amount of hydrogen entering the silicon substrate is the key factor for the extent of observable LeTID, this is an indication that AlO_x acts as a diffusion barrier for hydrogen originating from the SiN_y:H layer. Following this interpretation, the results imply a threshold thickness of about 15 nm at a firing set-peak temperature of 800°C, after which no more changes in LeTID behavior can be observed. This assumption is supported by a sample without a SiN_y:H capping layer (stars in Fig. 5), which shows comparable $\Delta N_{leq,max}$ values to the samples with a SiN_y:H capping layer.

To further exclude any influence of the varying deposition time during AlO_x deposition on LeTID, Groups B and C were investigated as well. Fig. 5 shows the maximum values of ΔN_{leq} reached during degradation of all investigated samples. As can be seen, samples from Group A (squares in Fig. 5) and Group B (circles in Fig. 5) reach comparable $\Delta N_{leq,max}$ values, thus showing that the AlO_x deposition time at 300°C does not significantly influence LeTID. Moreover, samples from Group C (triangles in Fig. 5) with an additional outgassing step at 400°C for 24 h also show comparable $\Delta N_{leq,max}$ values. Presuming that this outgassing step led to a lower H concentration in the AlO_x layer, a significant influence of the H content in the AlO_x layer on LeTID in the investigated layer system in combination with SiN_y:H can be excluded. Furthermore, FT-IR measurements of the AlO_x layers before and after the firing step did neither show detectable absorption between 2800 and 3900 cm^{-1} being characteristic to O–H and Al–H stretching modes [52]–[54] nor absorption at 2200 cm^{-1} corresponding to the Si–H vibration mode [45], [55]. Consistent with literature [41], this indicates a quite low H content in the ALD AlO_x layer deposited at 300°C, which therefore has no or only a weak impact on LeTID kinetics.

Even though $\Delta N_{leq,max}$ values differ roughly by one order of magnitude, the described observations hold true for both mc and Cz-Si (blue and orange symbols in Fig. 5). In order to verify the hypothesis of AlO_x being an effective diffusion barrier layer for hydrogen from a SiN_y:H capping layer, a detailed diffusion analysis is necessary and described in the following section.

B. Hydrogen/Deuterium Diffusion Analysis

So far, all investigations regarding hydrogen diffusion through AlO_x layers were done by indirect measurements or evidence [34], [40]. SIMS measurements after the firing step give direct insight into the barrier effect of the ALD AlO_x layer regarding deuterium diffusion. We presume here that the diffusion of hydrogen and deuterium is comparable (taking into account the different masses of hydrogen and deuterium), and therefore can deduce information on the link between hydrogen and LeTID.

Fig. 6 shows SIMS measurements of the deuterium in the vicinity of the c-Si/a-Si interface on the backside of the samples described in Section II.B, originating from the front SiN_y:D capping layer, thus having penetrated both the ALD AlO_x layer

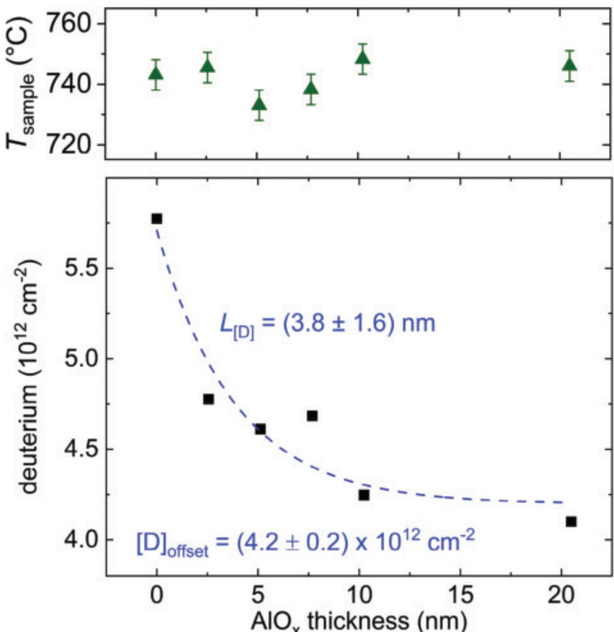

Fig. 7. Maximum sample temperature during firing of the AlO_x/SiN_y:D samples ($T_{set} = 850$°C) (top) with the systematic error of the temperature tracker and the thermoelement. Integrated deuterium concentration at the 40-nm-thick a-Si/c-Si interface (bottom). The dashed line is a single exponential fit to the measured data. Both graphs are plotted against the AlO_x thickness within the AlO_x/SiN_y:D layer system.

(variable thickness 0–20 nm) and the c-Si bulk (see Fig. 2). As can be seen, the deuterium concentration is below the SIMS detection limit in the c-Si bulk, and only in the vicinity of the c-Si/a-Si interface, the deuterium concentration starts to rise. Toward more negative *x*-axis values in the a-Si layer, the deuterium concentration drops again below the detection limit within approx. 500 nm (not shown in Fig. 6), which validates that 1.5 μm of a-Si are enough to completely absorb the deuterium penetrating the c-Si bulk. Moreover, no deuterium signal can be detected except for the region directly underneath the back side exposed the atmosphere during firing, meaning no deuterium is diffusing from the atmosphere through the a-Si layer to the a-Si/c-Si interface and thus could distort the results. However, as no correlation between AlO_x thickness and deuterium concentration in the a-Si layer could be found, the c-Si/a-Si interface was examined more closely.

AFM measurements show a surface roughness of approx. 40 nm on a FZ-Si wafer from the same batch after an HF dip (see inlay in Fig. 6). In addition, the SIMS crater might not be totally homogeneous in depth. Therefore, the interface roughness during the SIMS measurement is also assumed to be around 40 nm and is highlighted in gray in Fig. 6. To compare the total amount of deuterium in the interface region, the integral of the deuterium concentration [D] in the interface region was calculated and is plotted in Fig. 7 as a function of the AlO_x thickness. Without an AlO_x interlayer, we calculated a deuterium concentration of about $5.8 \times 10^{12}\mathrm{cm}^{-2}$. By adding a 2.5-nm-thick AlO_x interlayer, the deuterium concentration is already reduced to around $4.8 \times 10^{12}\mathrm{cm}^{-2}$ and can be lowered further with thicker interlayers. The lowest concentration of $4.1 \times 10^{12}\mathrm{cm}^{-2}$ is reached for a 20-nm-thick AlO_x layer. Fitting measured data by a single exponential decay function (dashed line in Fig. 7) results in a diffusion length of deuterium in the ALD AlO_x interlayer of $L_{[D]} = (3.8 \pm 1.6)$ nm. The sample peak temperatures during firing of the investigated samples are shown in the upper graph of Fig. 7. It can be seen that all sample peak temperatures are within the range of 730°C –750°C, with an arithmetic mean of (743 ± 2)°C.

Helmich *et al*. [40] determined diffusion lengths of hydrogen in ALD AlO_x by bulk resistivity measurements (here referred to as $L_{[H]}$) at different firing sample peak temperatures. From interpolation, a diffusion length of approx. 6.0 nm in their work is determined at a sample peak temperature of 743°C.

According to theories of diffusion based upon kinetic theory, the diffusion coefficient *D* is inversely proportional to the square root of the mass of the diffusing species [56]. Therefore, with $L \propto \sqrt{D}$, the expected ratio of the hydrogen diffusion length to that of deuterium is $\sqrt[4]{2} \approx 1.19$, which explains the lower diffusion length determined in this work compared to $L_{[H]}$ established by Helmich *et al*. [40].

Interestingly, the fit yields an offset value of $[D]_{offset} = (4.2 \pm 0.2) \times 10^{12}$ cm^{-2}. Helmich *et al.* [40] attributed this non-zero saturation (which was lower in their work) to a hydrogen content in the AlO_x layer itself diffusing into the c-Si bulk during the firing step. As the ALD AlO_x layers deposited in our work were not intentionally deuterated and the natural isotope ratio for deuterium is only at 0.015%, the here-observed offset cannot be attributed to the effect described in [40]. Furthermore, an in-diffusion from the back side of the wafer can be excluded because deuterium is below the detection limit in most of the a-Si layer bulk. To further investigate if these observations are a measurement artifact or of true nature, resistivity measurements were applied. By this, the concentration of BH pairs in the c-Si bulk can be determined, which can lead to the total hydrogen content therein [39]. To exclude any influence due to sample processing or firing temperature, wafers identically processed as for SIMS measurements were used. Since SiH_4, as well as ND_3, was used as precursors, the deuterated SiN_y:D layer contains both hydrogen and deuterium. Consequently, the doping effect can be negated by both species. As the resistivity measurement cannot distinguish between [BH] and [BD], the sum of both is determined.

Fig. 8 shows the sum of boron–hydrogen and boron–deuterium pair concentration as a function of the AlO_x interlayer thickness. It can be seen, that with increasing AlO_x thickness, [BH]+[BD] in the c-Si bulk decreases as well as the deuterium concentration at the a-S/c-Si interface (Fig. 7). Two single exponential decay fits were applied to the measured data, one with the diffusion length $L_{[D]}$ determined by the above-described SIMS measurement (blue dashed/dotted line) and the other with assuming no offset, leading to a diffusion length $L_{[H]+[D]} = 6.2$ nm (orange dashed line) with an error of $\pm$ 0.3 nm (fit error only). As can be seen, the fit with no offset matches the measured data better. This indicates that the neutralization of boron might be mostly caused by hydrogen, as the determined diffusion length of (6.2 ± 0.3) nm is close to the hydrogen diffusion length determined by Helmich *et al.* [40].

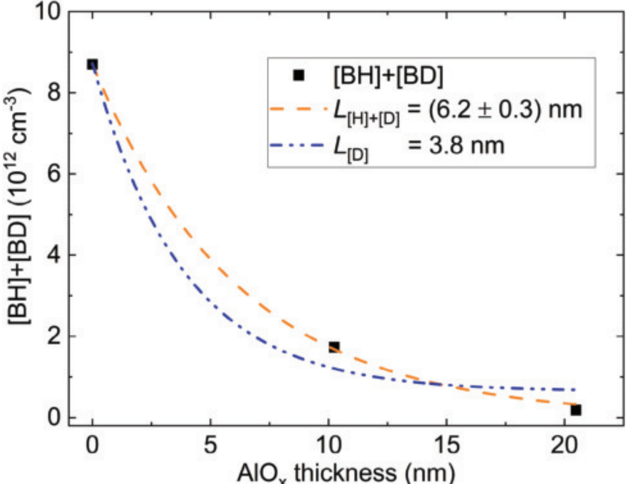

Fig. 8. [BH]+[BD] values of three investigated samples. Fitting with a single exponential function with assuming no offset (orange dashed line) and with the diffusion length $L_{[D]}$ (blue dashed/dotted line).

Furthermore, even when applying the diffusing length $L_{[D]}$, the offset value becomes very low and amounts to only $(0.64 \pm 0.53) \times 10^{12}\ \mathrm{cm}^{-3}$. In addition to the good matching fit with assuming no offset, this shows that the offset value determined by SIMS is either a measurement artifact or there is an unknown reason for deuterium to accumulate in the a-Si layer close to the interface. Since we cannot verify or reject either hypothesis, further experiments on this topic are necessary.

Nevertheless, both SIMS and resistivity measurement results indicate that ALD AlO_x serves as a highly effective diffusion barrier for H and D originating from the above SiN_y:H/D layer with a diffusion length of (3.8 ± 1.6) nm for deuterium (SIMS data) and (6.2 ± 0.3) nm for hydrogen plus deuterium (resistivity data), respectively.

Comparing these results with the findings in Section III-A, there is reason to presume that hydrogen is a key factor for the defect responsible for LeTID, which could be easily reduced by adding an AlO_x interlayer beneath the SiN_y:H capping layer.

IV. Conclusion

In conclusion, the influence of different AlO_x layer thicknesses in AlO_x/SiN_y:H layer systems on the extent of LeTID in p-type boron-doped mc-Si as well as in p-type Cz-Si using injection-dependent PCD measurements was investigated. We showed that thicker ALD AlO_x layers can effectively reduce the defect responsible for LeTID. This suggests a threshold thickness of AlO_x regarding hydrogen diffusing from the SiN_y:H capping layer through the AlO_x layer into the crystalline silicon bulk, which we confirmed by applying SIMS and resistivity measurements.

Direct measurements of deuterium concentrations showed that its in-diffusion can be reduced by adding an ALD AlO_x layer beneath the SiN_y:D layer, and the diffusion length of deuterium in AlO_x is determined to be (3.8 ± 1.6) nm at a firing temperature of (743 ± 2)°C. These observations were further confirmed by determining [BH]+[BD] via resistivity measurements. Moreover, they showed that the offset of the deuterium concentration observed by SIMS analysis is either a measurement artifact or due to an unknown effect at the a-Si/c-Si interface.

Considering hydrogen to be a main trigger for the defect responsible for LeTID, adapting the AlO_x layer thickness is an easy way to control ΔN_{leq} and could help to understand the LeTID causing defect better and might even lead to a more detailed analysis of its formation dynamics.

Acknowledgment

The authors would like to thank L. Mahlstaedt, B. Rettenmaier and U. Wohlert for technical support, M. Heilig for AFM measurements, and F. Geml for supporting discussions.

References

[1] F. Kersten *et al.*, "Degradation of multicrystalline silicon solar cells and modules after illumination at elevated temperature," *Sol. Energy Mater. Sol. Cells*, vol. 142, pp. 83–86, 2015.

[2] K. Ramspeck *et al.*, "Light induced degradation of rear passivated mc-si solar cells," in *Proc. 27th Eur. Photovolt. Sol. Energy Conf. Exhib.*, Frankfurt, Germany, 2012, pp. 861–865.

[3] A. Zuschlag, D. Skorka, and G. Hahn, "Degradation and regeneration analysis in mc-Si," in *Proc. IEEE 43rd Photovolt. Specialists Conf.*, 2016, pp. 1051–1054.

[4] D. Bredemeier, D. Walter, S. Herlufsen, and J. Schmidt, "Lifetime degradation and regeneration in multicrystalline silicon under illumination at elevated temperature," *AIP Adv.,* vol. 6, 2016, Art. no. 035119.

[5] J. Lindroos and H. Savin, "Review of light-induced degradation in crystalline silicon solar cells," *Sol. Energy Mater. Sol. Cells*, vol. 147, pp. 115–126, 2016.

[6] J. M. Fritz, A. Zuschlag, D. Skorka, A. Schmid, and G. Hahn, "Temperature dependent degradation and regeneration of differently doped mc-Si materials," *Energy Procedia*, vol. 124, pp. 718–725, 2017.

[7] D. Sperber, A. Heilemann, A. Herguth, and G. Hahn, "Temperature and light-induced changes in bulk and passivation quality of boron-doped float-zone silicon coated with SiN_x:H," *IEEE J. Photovolt.*, vol. 7, no. 2, pp. 463–470, Mar. 2017.

[8] D. Chen *et al.*, "Evidence of an identical firing-activated carrier-induced defect in monocrystalline and multicrystalline silicon," *Sol. Energy Mater. Sol. Cells*, vol. 172, pp. 293–300, 2017.

[9] F. Fertig *et al.*, "Mass production of p-type Cz silicon solar cells approaching average stable conversion efficiencies of 22%," *Energy Procedia*, vol. 124, pp. 338–345, 2017.

[10] T. Niewelt, M. Selinger, N. E. Grant, W. Kwapil, J. D. Murphy, and M. C. Schubert, "Light-induced activation and deactivation of bulk defects in boron-doped float-zone silicon," *J. Appl. Phys.*, vol. 121, 2017, Art. no. 185702.

[11] A. Graf, A. Herguth, and G. Hahn, "Determination of BO-LID and LeTID related activation energies in Cz-Si and FZ-Si using constant injection conditions," in *Proc. AIP Conf.*, 2019, Art. no. 140003.

[12] A. Zuschlag, D. Skorka, and G. Hahn, "Degradation and regeneration in mc-Si after different gettering steps," *Prog. Photovolt. Res. Appl.*, vol. 25, pp. 545–552, 2017.

[13] R. Eberle, W. Kwapil, F. Schindler, M. C. Schubert, and S. W. Glunz, "Impact of the firing temperature profile on light induced degradation of multicrystalline silicon," *Physica Status Solidi RRL*, vol. 10, pp. 861–865, 2016.

[14] T. Niewelt, F. Schindler, W. Kwapil, R. Eberle, J. Schön, and M. C. Schubert, "Understanding the light-induced degradation at elevated temperatures: Similarities between multicrystalline and floatzone p-type silicon," *Prog. Photovolt. Res. Appl.*, vol. 26, pp. 533–542, 2018.

[15] C. E. Chan *et al.*, "Rapid stabilization of high-performance multicrystalline p-type silicon PERC cells," *IEEE J. Photovolt.*, vol. 6, no. 6, pp. 1473–1479, Nov. 2016.

[16] C. Vargas *et al.*, "Carrier-induced degradation in multicrystalline silicon: Dependence on the silicon nitride passivation layer and hydrogen released during firing," *IEEE J. Photovolt.*, vol. 8, no. 2, pp. 413–420, Mar. 2018.

[17] D. Bredemeier, D. C. Walter, R. Heller, and J. Schmidt, "Impact of hydrogen-rich silicon nitride material properties on light-induced lifetime degradation in multicrystalline silicon," *Physica Status Solidi RRL*, vol. 13, 2019, Art. no. 1900201.

[18] J. Schmidt, D. Bredemeier, and D. C. Walter, "On the defect physics behind light and elevated temperature-induced degradation (LeTID) of multicrystalline silicon solar cells," *IEEE J. Photovolt.*, vol. 9, no. 6, pp. 1497–1503, Nov. 2019.

[19] T. H. Fung *et al.*, "A four-state kinetic model for the carrier-induced degradation in multicrystalline silicon: Introducing the reservoir state," *Sol. Energy Mater. Sol. Cells*, vol. 184, pp. 48–56, 2018.

[20] K. Nakayashiki *et al.*, "Engineering solutions and root-cause analysis for light-induced degradation in p-type multicrystalline silicon PERC modules," *IEEE J. Photovolt.*, vol. 6, no. 4, pp. 860–868, Jul. 2016.

[21] D. Chen *et al.*, "Hydrogen induced degradation: A possible mechanism for light- and elevated temperature induced degradation in n-type silicon," *Sol. Energy Mater. Sol. Cells*, vol. 185, pp. 174–182, 2018.

[22] A. Ciesla née Wenham *et al.*, "Hydrogen-induced degradation," in *Proc. IEEE 7th World Conf. Photovolt. Energy Convers.*, Waikoloa Village, HI, USA, 2018, pp. 0001–0008.

[23] S. Liu *et al.*, "Impact of dark annealing on the kinetics of light- and elevated-temperature-induced degradation," *IEEE J. Photovolt.*, vol. 8, no. 6, pp. 1494–1502, Nov. 2018.

[24] D. Bredemeier, D. C. Walter, and J. Schmidt, "Possible candidates for impurities in mc-Si wafers responsible for light-induced lifetime degradation and regeneration," *Sol. RRL*, vol. 2, 2018, Art. no. 1700159.

[25] A. E. Morishige *et al.*, "Lifetime spectroscopy investigation of light-induced degradation in p-type multicrystalline silicon PERC," *IEEE J. Photovolt.*, vol. 6, no. 6, pp. 1466–1472, Nov. 2016.

[26] C. Vargas *et al.*, "Influence of silicon nitride and its hydrogen content on carrier-induced degradation in multicrystalline silicon," in *Proc. 33rd Eur. Photovolt. Sol. Energy Conf. Exhib.*, Amsterdam, The Netherlands, 2017, pp. 561–564.

[27] H. Deniz, J. Bauer, and O. Breitenstein, "Nickel precipitation in light and elevated temperature degraded multicrystalline silicon solar cells," *Sol. RRL*, vol. 2, 2018, Art. no. 1800170.

[28] M. A. Jensen *et al.*, "Evaluating root cause: The distinct roles of hydrogen and firing in activating light- and elevated temperature-induced degradation," *J. Appl. Phys.*, vol. 124, 2018, Art. no. 085701.

[29] M. Wagner *et al.*, "Correlation of the LeTID amplitude to the aluminium bulk concentration and oxygen precipitation in PERC solar cells," *Sol. Energy Mater. Sol. Cells*, vol. 187, pp. 176–188, 2018.

[30] A. Schmid, A. Zuschlag, D. Skorka, J. Fritz, C. Winter, and G. Hahn, "Influence of different transition metal contaminations on degradation and regeneration in mc-Si," in *Proc. 33rd Eur. Photovolt. Sol. Energy Conf. Exhib.*, Amsterdam, The Netherlands, 2017, pp. 321–324.

[31] T. H. Fung *et al.*, "Influence of bound hydrogen states on carrier-induced degradation in multi-crystalline silicon," in *Proc. AIP Conf.*, 2018, vol. 1999, Art. no. 130004.

[32] D. Bredemeier, D. C. Walter, and J. Schmidt, "Lifetime degradation in multicrystalline silicon under illumination at elevated temperature: Indications for the involvement of hydrogen," in *Proc. AIP Conf.*, 2018, vol. 1999, Art. no. 130001.

[33] A. Schmid, J. Lindroos, A. Zuschlag, D. Skorka, J. Fritz, and G. Hahn, "Influence of low-temperature annealing before firing on LeTID in multicrystalline silicon," in *Proc. 35th Eur. Photovolt. Sol. Energy Conf. Exhib.*, Brussels, Belgium, 2018, pp. 342–345.

[34] U. Varshney *et al.*, "Controlling light- and elevated-temperature-induced degradation with thin film barrier layers," *IEEE J. Photovolt.*, vol. 10, no. 1, pp. 19–27, Jan. 2020.

[35] A. Schmid, C. Fischer, D. Skorka, A. Zuschlag, and G. Hahn, "Reducing LeTID with an adjustment of the AlO_x-SiN_y:H layer system," in *Proc. 37th Eur. Photovolt. Sol. Energy Conf. Exhib., Online Conf.*, 2020, pp. 156–159.

[36] S. Wilking, A. Herguth, and G. Hahn, "Influence of hydrogen on the regeneration of boron-oxygen related defects in crystalline silicon," *J. Appl. Phys.*, vol. 113, 2013, Art. no. 194503.

[37] A. A. Dameron, S. D. Davidson, B. B. Burton, P. F. Carcia, R. S. McLean, and S. M. George, "Gas diffusion barriers on polymers using multilayers fabricated by Al_2O_3 and rapid SiO_2 atomic layer deposition," *J. Phys. Chem. C*, vol. 112, pp. 4573–4580, 2008.

[38] V. V. Voronkov and R. Falster, "Formation, dissociation, and diffusion of various hydrogen dimers in silicon," *Phys. Status Solidi B*, vol. 254, 2017, Art. no. 1600779.

[39] D. C. Walter, D. Bredemeier, R. Falster, V. V. Voronkov, and J. Schmidt, "Easy-to-apply methodology to measure the hydrogen concentration in boron-doped crystalline silicon," *Sol. Energy Mater. Sol. Cells*, vol. 200, 2019, Art. no. 109970.

[40] L. Helmich, D. C. Walter, D. Bredemeier, and J. Schmidt, "Atomic-layer-deposited Al_2O_3 as effective barrier against the diffusion of hydrogen from SiNx:H layers into crystalline silicon during rapid thermal annealing," *Physica Status Solidi RRL*, vol. 14, 2020, Art. no. 2000367.

[41] J. van Hemmen *et al.*, "Plasma and thermal ALD of Al_2O_3 in a commercial 200 mm ALD reactor," *J. Electrochem. Soc.*, vol. 154, pp. 165–169, 2007.

[42] R. A. Sinton and A. Cuevas, "Contactless determination of current–voltage characteristics and minority-carrier lifetimes in semiconductors from quasi-steady-state photoconductance data," *Appl. Phys. Lett.*, vol. 69, no. 17, pp. 2510–2512, 1996.

[43] A. Herguth, "On the meaning(fullness) of the intensity unit 'suns' in light induced degradation experiments," *Energy Procedia*, vol. 124, pp. 53–59, 2015.

[44] A. Herguth, "On the lifetime-equivalent defect density: Properties, application, and pitfalls," *IEEE J. Photovolt.*, vol. 9, no. 5, pp. 1182–1194, Sep. 2017.

[45] V. Verlaan, C. H. M. van der Werf, W. M. Arnoldbik, H. D. Goldbach, and R. E. I. Schropp, "Unambiguous determination of Fourier-transform infrared spectroscopy proportionality factors: The case of silicon nitride," *Phys. Rev. B*, vol. 73, 2006, Art. no. 195333.

[46] W. A. Lanford and M. J. Rand, "The hydrogen content of plasma-deposited silicon nitride," *J. Appl. Phys.*, vol. 49, pp. 2473–2477, 1978.

[47] S. Gerke, G. Hahn, R. Job, and B. Terheiden, "Bias-plasma assisted RF magnetron sputter deposition of hydrogen-less amorphous silicon," *Energy Procedia*, vol. 84, pp. 105–109, 2015.

[48] M. Sheoran *et al.*, "Hydrogen diffusion in silicon from PECVD silicon nitride," in *Proc. IEEE 33rd Photovolt. Specialists Conf.*, 2008, pp. 1–4.

[49] S. J. Pearton, J. W. Corbett, and T. S. Shi, "Hydrogen in crystalline semiconductors," *Appl. Phys. A*, vol. 43, pp. 153–195, 1987.

[50] A. Herguth and C. Winter, "Quantifying boron–hydrogen pairs in crystalline silicon by means of direct resistance measurements," *IEEE J. Photovolt.*, to be published, doi: 10.1109/JPHOTOV.2021.3074463.

[51] J. Lindroos, A. Zuschlag, D. Skorka, and G. Hahn, "Silicon nitride deposition: Impact on lifetime and light-induced degradation at elevated temperature in multicrystalline silicon," *IEEE J. Photovolt.*, vol. 10, no. 1, pp. 8–18, Jan. 2020.

[52] V. Verlaan, L. R. van den Elzen, G. Dingemans, M. C. M. van de Sanden, and W. M. M. Kessels, "Composition and bonding structure of plasma-assisted ALD Al_2O_3 films," *Phys. Status Solidi C*, vol. 7, pp. 976–979, 2010.

[53] W. Liang, D. Suh, J. Yu, J. Bullock, and K. J. Weber, "Degradation of the surface passivation of plasma-assisted ALD Al_2O_3 under damp-heat exposure," *Phys. Status Solidi A*, vol. 212, pp. 274–281, 2015.

[54] G. Kaur *et al.*, "Understanding surface treatment and ALD AlO_x thickness induced surface passivation quality of c-Si Cz wafers," *IEEE J. Photovolt.*, vol. 7, no. 5, pp. 1224–1235, Sep. 2017.

[55] H. Goverde *et al.*, "Al_2O_3 surface passivation characterized on hydrophobic and hydrophilic c-Si by a combination of QSSPC, CV, XPS, and FTIR," *Energy Procedia*, vol. 27, pp. 355–360, 2012.

[56] W. T. Kelvin, "Lecture XVII," in *Baltimore Lectures on Molecular Dynamics and the Wave Theory of Light*, Cambridge, U.K.: Cambridge Univ. Press, 1904, pp. 279–323.